Journal of Coordination Chemistry
Publication details, including instructions for authors and subscription information:
http://www.tandfonline.com/loi/gcoo20

Preparation and characterization of two new 2-D double helical networks based on 1,3-bis(4-pyridyl)propane

Lijuan Zhang [a], Donghua Xu [a], Yunshan Zhou [a], Yan Guo [a] & Waqar Ahmad [a]

[a] State Key Laboratory of Chemical Resource Engineering, College of Science, Beijing University of Chemical Technology, Beijing 100029, P. R. China

Accepted author version posted online: 02 Jul 2012.Published online: 18 Jul 2012.

To cite this article: Lijuan Zhang, Donghua Xu, Yunshan Zhou, Yan Guo & Waqar Ahmad (2012) Preparation and characterization of two new 2-D double helical networks based on 1,3-bis(4-pyridyl)propane, Journal of Coordination Chemistry, 65:17, 3028-3039, DOI: 10.1080/00958972.2012.708410

To link to this article: http://dx.doi.org/10.1080/00958972.2012.708410

Journal of Coordination Chemistry
Vol. 65, No. 17, 10 September 2012, 3028–3039

Preparation and characterization of two new 2-D double helical networks based on 1,3-bis(4-pyridyl)propane

LIJUAN ZHANG, DONGHUA XU, YUNSHAN ZHOU*, YAN GUO and WAQAR AHMAD

State Key Laboratory of Chemical Resource Engineering, College of Science, Beijing University of Chemical Technology, Beijing 100029, P. R. China

(*Received 18 March 2012; in final form 25 May 2012*)

Two new coordination polymers, $[Zn(p\text{-}CH_3C_6H_5SO_3)_2(bpp)_2]_n$ (**1**) and $[Cu_2(SCN)_2(NO_3)_2(bpp)_4]_n$ (**2**) (bpp = 1,3-bis(4-pyridyl)propane), have been synthesized and characterized. Single crystal X-ray diffraction analysis reveals that **1** and **2** exhibit 2-D layer networks composed of alternate left-handed and right-handed bpp-containing helical chains by sharing Zn(II) in **1** and Cu(II) in **2**. Compound **1** exhibits a 2-D undulated double-helical network, while **2** shows a two-fold interpenetrated 2-D double-helical network. *p*-Toluene sulfonates select Zn^{2+} rather than Cu^{2+} to coordinate, while both SCN^- and NO_3^- select Cu^{2+} rather than Zn^{2+}, indicating that the specific organic ligand shows preference/selectivity when different types of metal ions are concurrently present. As a consequence, anionic ligands of different structures impose remarkable influence on the structures of the resultant compounds. Compound **1** shows a broad peak at 415 nm in its emission spectrum, indicating an efficient energy transfer.

Keywords: Double helical networks; Interpenetration; Preparation; Transition metal compounds

1. Introduction

Helical coordination polymers have potential applications in chiral separations, asymmetric catalysis and nonlinear optics [1–4]. A promising strategy for construction is the assembly of small components into extended polymeric materials [1]. Versatile ligands that can bind to several metal centers and direct the assembly into extended coordination polymers with desired helical structures and properties are necessary [5, 6]. Previous studies have shown that flexible ligands can fulfill the requirement [7]; for example, a large number of 1-D helical chains, 2-D helical layers, and 3-D helical metal-organic coordination polymers [3b, 6d, 8–11] have been synthesized by using flexible organic ligands [1e, 3b, 6d, 8–11].

Among various flexible organic ligands, we are interested in 1,3-bis(4-pyridyl)propane (bpp) ligand for the construction of helical frameworks [12] because bpp possesses flexibility and functionality due to three methylene groups between the two 4-pyridyl

*Corresponding author. Email: zhouys@mail.buct.edu.cn

Journal of Coordination Chemistry
ISSN 0095-8972 print/ISSN 1029-0389 online
http://dx.doi.org/10.1080/00958972.2012.708410

rings in contrast to 4,4′-bipyridyl homologues [13]. Due to varying orientations of methylene groups, bpp can adopt different ligand conformations, such as TT, TG, GG, and GG′ (T = *trans* and G = gauche) [14]. Some polymers based on bpp have been reported, all featuring helical structures [15–17]. Besides the ability to form helical structures, bpp can construct interpenetrated structures through the assembly process with metal cations. Many bpp-based metal-organic coordination polymers show interpenetrated structures [15a, 18]. However, coordination polymers possessing both helical and interpenetrated structures are rare [1e, 15a], and the design and synthesis of helical coordination polymers with interpenetrated structures is still a challenge for crystal engineering.

By carefully comparing the bpp-based metal-organic coordination polymers featuring either helical or interpenetrating characters, it was noticed that size, type, and configuration of anionic ligands often impose decisive influence on the resultant helical and/or interpenetrated structures [15–18]. However, influence from anionic ligands still needs systematic studies to en route the rational design and construction of bpp-containing helical structures.

In order to investigate the synthetic regularity and influence of anionic ligands on the structures, bpp was chosen to react with Cu(II) or Zn(II) salts in the presence of *p*-toluenesulfonate, NO_3^- and NSC^-, which are different with respect to their size and configuration. As a consequence, two new 2-D helical coordination polymers, $[Zn(p\text{-}CH_3C_6H_4SO_3)_2(bpp)_2]_n$ (**1**) and $[Cu_2(SCN)_2(NO_3)_2(bpp)_4]_n$ (**2**), were obtained. In this article, the syntheses, characterizations, structures and properties of the two new polymers are reported.

2. Experimental

2.1. *Materials and equipment*

All materials were of reagent grade, obtained from commercial sources, and used without purification. Elemental analyses for C, H, and N were performed on a Perkin-Elmer 240C analytical instrument. IR spectra were recorded on a Nicolet FTIR-170SX spectrophotometer as KBr pellets from 4000 to 400 cm^{-1}. Thermogravimetric analysis was carried out on a NETZSCH STA 449C unit at a heating rate of 5°C min^{-1}. Excitation and emission spectra were measured with a Hitachi F-7000FL fluorescence spectrophotometer with both excitation and emission slits of 2.5 nm for **1** in the solid state using a xenon arc lamp (150w). Powder X-ray diffraction (XRD) measurements were performed on a Rigaku-Dmax 2500 diffractometer at a scanning rate of 15° min^{-1} in the 2θ range from 5° to 50°, with graphite monochromated Cu-Kα radiation ($\lambda = 0.15405$ nm).

2.2. *Syntheses of 1 and 2*

2.2.1. Synthesis of 1. To a solution of $Zn(NO_3)_2 \cdot 6H_2O$ (0.25 mmol, 0.074 g) and sodium *p*-toluenesulfonate (0.5 mmol, 0.098 g) in 8 mL of distilled water, bpp (0.25 mmol, 0.050 g) in 8 mL ethanol was added dropwise under stirring. After stirring

for 1 h, the solution was filtered and the filtrate was left undisturbed at room temperature for crystallization. After 3 days, colorless block crystals were harvested from the filtrate with a yield of 0.073 g (72.6% based on bpp). Anal. Calcd for $C_{40}H_{42}N_4O_6S_2Zn$ (%): C, 59.73; H, 5.26; N, 6.97. Found (%): C, 59.68; H, 5.22; N, 6.96. Fourier transform IR (KBr, cm^{-1}): 3442(w), 3086(w), 2962(w), 2889(w), 1626(s), 1431(s), 1261(s), 1194(vs), 1044(s), 822(m), and 570(m).

2.2.2. Synthesis of 2. To a solution of NH_4SCN (3 mmol, 0.228 g) in 10 mL of methanol, $Cu(NO_3)_2 \cdot 3H_2O$ (1 mmol, 0.242 g) in 5 mL of methanol was added dropwise under stirring. The resultant solution was stirred for 5 min, and then 5 mL of a methanol solution containing bpp (2 mmol, 0.396 g) was added, resulting instantly in a large amount of grass green solid precipitates. DMF (35 mL) was added dropwise to completely dissolve the green precipitates, then the solution was stirred for further 0.5 h, filtered, and left undisturbed at room temperature. Dark blue block crystals were harvested after 5 days from the mother solution with a yield of 0.475 g (82.1% based on bpp). Anal. Calcd for $C_{54}H_{54}Cu_2N_{12}O_6S_2$ (%): C, 55.99; H, 4.69; N, 14.51. Found (%): C, 55.94; H, 4.66; N, 14.50. Fourier transform FT-IR (KBr, cm^{-1}): 3430(m), 3081(w), 2938(w), 2866(w), 2056(s), 1620(vs), 1560(w), 1386(vs), 1314(s), 1071(m), 810(m), and 516(m).

2.3. *X-ray structure analyses*

Diffraction intensities for **1** and **2** were collected at 293(2) K on a computer-controlled Bruker APEXII CCD area-detector equipped with graphite monochromated Mo-Kα, with a radiation wavelength of 0.71073 Å using the ω-scan technique. The structures were solved by direct methods and refined with full-matrix least squares using the SHELXS-97 and SHELXL-97 programs [19].

Anisotropic thermal parameters were assigned to all non-hydrogen atoms. Organic hydrogen atoms were set in calculated positions and refined as riding with a common fixed isotropic thermal parameter. The crystal data and refinements of **1** and **2** are summarized in table 1. Selected bond lengths and angles for **1** and **2** are listed in table 2 (Supplementary material).

3. Results and discussion

3.1. *Descriptions of the structures*

3.1.1. Crystal structure of 1. Compound **1** crystallizes in the orthorhombic system, space group *Pnna*. The asymmetric unit of **1** contains one crystallographically independent Zn(II), one *p*-toluenesulfonate, and one bpp (figure 1). Each Zn(II) is six-coordinate with four nitrogen atoms from four different bpp and two oxygen atoms from two different *p*-toluenesulfonates. Zn(II) is octahedral with bond distances of 2.1916(18) Å for Zn1–N1, 2.2092(19) Å for Zn1–N2, and 2.1983(18) Å for Zn1–O2, respectively. The O–Zn–N, O–Zn–O, and N–Zn–N bond angles vary from 85.93(10)° to 178.79(6)°. All bond lengths and angles in **1** are within the normal ranges and conform

Table 1. Crystallographic data for **1** and **2**.

Compound	**1**	**2**
Empirical formula	$C_{40}H_{42}N_4O_6S_2Zn$	$C_{54}H_{54}Cu_2N_{12}O_6S_2$
Formula weight	804.27	1158.29
Crystal system	Orthorhombic	Monoclinic
Space group	*Pnna*	*P2(1)/n*
Unit cell dimensions (Å, °)		
a	23.900(5)	18.140(4)
b	17.290(4)	16.170(3)
c	9.3100(19)	20.660(4)
α	90	90
β	90	114.05(3)
γ	90	90
Volume (Å^3), *Z*	3847.2(13), 4	5534.0(19), 4
Calculated density (Mg m^{-3})	1.389	1.390
Absorption coefficient (mm^{-1})	0.799	0.904
F(000)	1680	2400
Goodness-of-fit on F^2	1.000	1.003
Final *R* indices [$I > 2\sigma(I)$][a]	$R_1 = 0.0390$	$R_1 = 0.0609$
R indices (all data)[b]	$wR_2 = 0.1501$	$wR_2 = 0.1237$
Largest difference peak and hole (e Å^{-3})	0.674 and −0.700	0.490 and −0.363

[a] $R_1 = \Sigma||F_o| - |F_c||/\Sigma|F_o|$.
[b] $wR_2 = \Sigma[w(F_o^2 - F_c^2)^2]/\Sigma[w(F_o^2)^2]^{1/2}$.

Table 2. Selected bond lengths and angles for **1** and **2**.

1			
N(1)–Zn(1)	2.1916(18)	Zn(1)–N(1)#3	2.1916(18)
N(2)–Zn(1)	2.2092(19)	Zn(1)–O(2)#3	2.1983(18)
O(2)–Zn(1)	2.1983(18)	Zn(1)–N(2)#3	2.2092(19)
N(1)–Zn(1)–N(1)#3	86.69(10)	N(1)#3–Zn(1)–N(2)#3	93.70(7)
N(1)–Zn(1)–O(2)	89.76(7)	O(2)–Zn(1)–N(2)#3	91.38(7)
N(1)#3–Zn(1)–O(2)	91.15(7)	O(2)#3–Zn(1)–N(2)#3	87.70(7)
N(1)–Zn(1)–O(2)#3	91.15(7)	N(1)–Zn(1)–N(2)	93.70(7)
N(1)#3–Zn(1)–O(2)#3	89.76(7)	O(2)–Zn(1)–N(2)	87.70(7)
O(2)–Zn(1)–O(2)#3	178.75(9)	O(2)#3–Zn(1)–N(2)	91.38(7)
N(1)–Zn(1)–N(2)#3	178.79(6)	N(2)#3–Zn(1)–N(2)	85.93(10)
2			
Cu(1)–O(1)	2.636(25)	Cu(2)–O(4)	2.645(17)
Cu(1)–N(1)	2.021(4)	Cu(2)–N(8)	2.030(4)
Cu(1)–N(4)	2.026(4)	Cu(2)–N(7)	2.039(5)
Cu(1)–N(3)	2.033(4)	Cu(2)–N(5)	2.051(5)
Cu(1)–N(2)	2.046(4)	Cu(2)–N(6)	2.039(4)
Cu(1)–N(9)	2.419(6)	Cu(2)–N(10)	2.363(6)
N(1)–Cu(1)–N(4)	90.34(17)	N(8)–Cu(2)–N(7)	91.20(18)
N(1)–Cu(1)–N(3)	176.20(19)	N(8)–Cu(2)–N(5)	87.41(18)
N(4)–Cu(1)–N(3)	89.49(17)	N(7)–Cu(2)–N(5)	174.52(19)
N(1)–Cu(1)–N(2)	92.85(17)	N(8)–Cu(2)–N(6)	176.71(19)
N(4)–Cu(1)–N(2)	176.12(17)	N(7)–Cu(2)–N(6)	90.62(18)
N(3)–Cu(1)–N(2)	87.18(17)	N(5)–Cu(2)–N(6)	90.53(18)
N(1)–Cu(1)–N(9)	90.83(19)	N(8)–Cu(2)–N(10)	91.24(18)
N(4)–Cu(1)–N(9)	93.5(2)	N(7)–Cu(2)–N(10)	93.62(18)
N(3)–Cu(1)–N(9)	92.96(19)	N(5)–Cu(2)–N(10)	91.71(18)
N(2)–Cu(1)–N(9)	88.66(18)	N(6)–Cu(2)–N(10)	91.38(19)
O(1)–Cu(1)–N(1)	88.386(173)	O(4)–Cu(2)–N(5)	85.835(184)
O(1)–Cu(1)–N(2)	87.836(171)	O(4)–Cu(2)–N(6)	92.268(179)
O(1)–Cu(1)–N(3)	87.847(173)	O(4)–Cu(2)–N(7)	88.752(183)
O(1)–Cu(1)–N(4)	90.024(171)	O(4)–Cu(2)–N(8)	85.020(179)
O(1)–Cu(1)–N(9)	176.380(171)	O(4)–Cu(2)–N(10)	175.607(171)

Symmetry transformations used to generate equivalent atoms. For **1**: #3 $-x+1, -y+1, -z+1$.

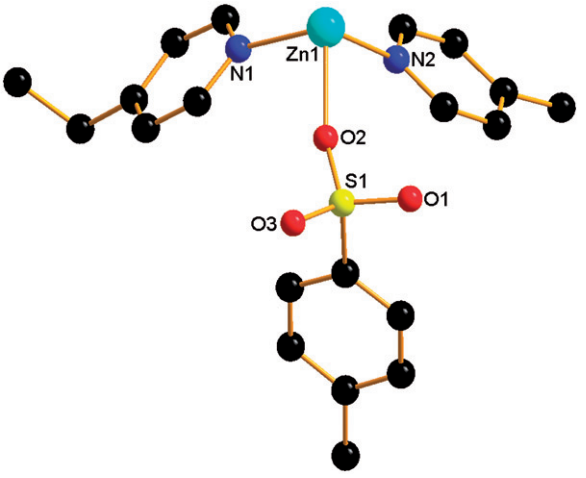

Figure 1. (Color online) View of the asymmetric unit in **1**. Hydrogen atoms were deleted for clarity. Color code: Zn, cyan; O, red; N, blue; C, black and S, yellow.

to those described in the literature [20]. The two oxygen atoms are apical and four nitrogen atoms are situated at the basal plane.

In **1**, bpp adopts TG conformation with N-to-N distance being 9.16 Å. As shown in figure 2(a), neighboring Zn(II) ions are interconnected *via* nitrogen atoms of bpp forming 1-D left-handed and right-handed helical chains, both with a screw pitch of *ca* 9.3 Å along the crystallographic 2_1 screw axis. Adjacent left-handed and right-handed helical chains then assemble alternately through sharing Zn(II) ions into a 2-D undulated helical layer. In the layer, four bpp ligands and four Zn(II) ions form a repeating regular rhombic grid with a side length of 12.82 Å based on the Zn···Zn distance, ∠Zn–Zn–Zn angles of 42.6° and 137.4° (figure 2b).

3.1.2. Crystal structure of 2. Compound **2** crystallizes in the monoclinic system, space group *P2(1)/n*. As shown in figure 3, in one asymmetric unit there are two crystallographically independent Cu(II) ions, four bpp, two NO_3^-, and two NSC^-. Each Cu1 and Cu2 is six-coordinate with four nitrogen atoms from four different bpp, one nitrogen atom from a NSC^- and one oxygen atom from NO_3^-. The distances of Cu1–N are 2.021(4) Å for (Cu1–N1), 2.046(4) Å for (Cu1–N2), 2.033(4) Å for (Cu1–N3), 2.026(4) Å for (Cu1–N4), and 2.419(6) Å for (Cu1–N9). The distances of Cu2–N are 2.051(5) Å for (Cu2–N5), 2.039(4) Å for (Cu2–N6), 2.039(5) Å for (Cu2–N7), 2.030(4) Å for (Cu2–N8), and 2.363(6) Å for (Cu2–N10). The distances of Cu–O are 2.636(25) Å for (Cu1–O1) and 2.645(17) Å for (Cu2–O4). The O–Cu–N and N–Cu–N bond angles vary from 85.020(179)° to 176.380(171)° and 87.18(17)° to 176.71(19)°, respectively. All bond lengths and angles in **2** are within the normal range and conform to those described in [21].

The four bpp in an asymmetric unit adopt three different conformations: both the N2/N3- and N1/N4-containing bpp linking Cu1 adopt GG′ and TG conformations with N-to-N distances of 8.27 and 9.13 Å, respectively, while both N6/N7- and N5/N8-containing bpp connecting Cu2 adopt TT and GG′ conformations with N-to-N

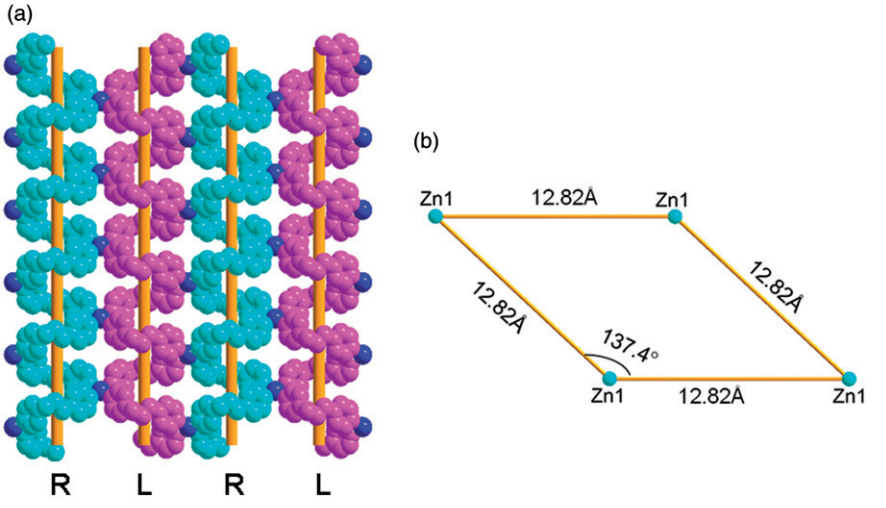

Figure 2. (Color online) View of the space-filling plot of the 2-D layer composed of left-handed (in pink) and right-handed (in cyan) helical double chains (blue balls stand for Zn ions) in **1** (a); the simplified repeating grid in the 2-D layer with labeled side lengths and angles in **1** (b). All H atoms and *p*-toluenesulfonates are omitted for clarity.

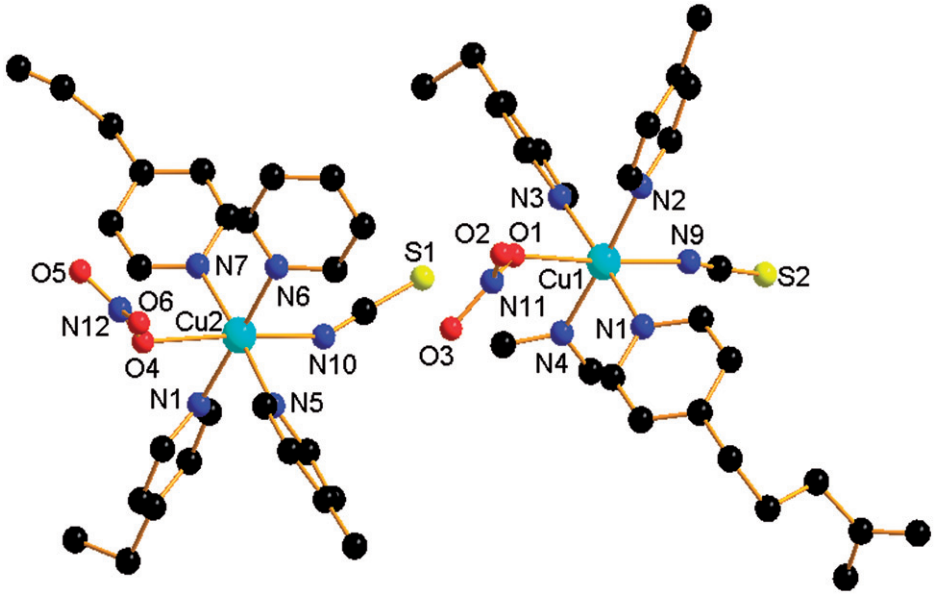

Figure 3. (Color online) Asymmetric unit in **2**. Hydrogen atoms are deleted for clarity.

distances of 9.44 and 8.14 Å, respectively. As shown in figure 4(a), neighboring Cu2 ions are interconnected *via* nitrogen atoms of bpp forming 1-D left-handed and right-handed helical chains, both with a pitch of *ca* 9.3 Å. Adjacent left-handed and right-handed helical chains are then assembled alternately through sharing Cu2 ions into a 2-D undulated helical layer (denoted Cu2-bpp layer). Like the situation for Cu2,

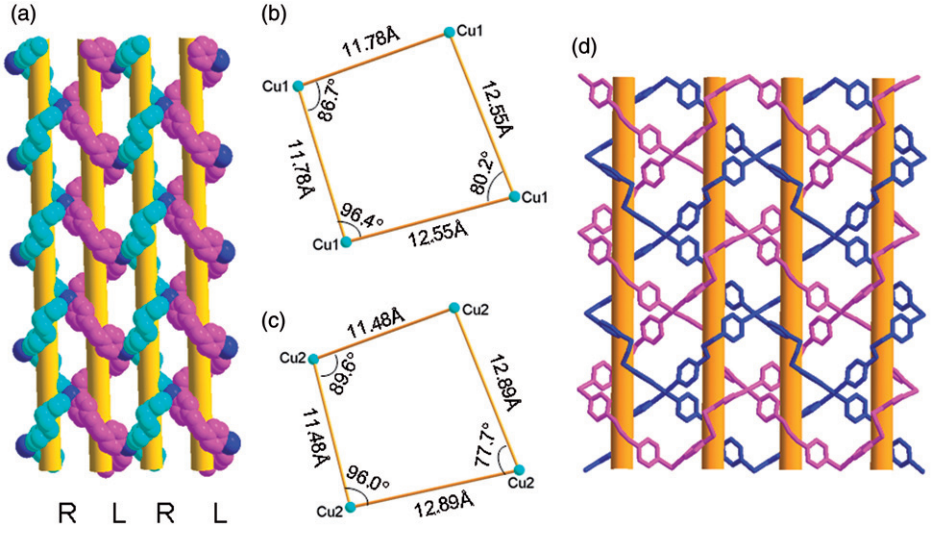

Figure 4. (Color online) View of the space-filling plot of the 2-D layer (Cu2-bpp layer) in **2** composed of left-handed (in pink) and right-handed (in cyan) double helical chains (a); view of the repeating irregular quadrilateral of the 2-D Cu1-bpp layer in **2** (b); view of the repeating irregular quadrilateral of the 2-D Cu2-bpp layer in **2** (c); view of two-fold interpenetrated layer structure of **2** (Cu1-bpp layer in pink, Cu2-bpp layer in blue) (d). Hydrogen atoms, NCS^-, and NO_3^- are omitted for clarity.

neighboring Cu1 ions also produce a 2-D undulated helical layer (denoted Cu1-bpp layer) composed of 1-D left-handed and right-handed helical chains, both with a pitch of *ca* 9.3 Å. Both the Cu1-bpp layer and Cu2-bpp layer can be simplified as 2-D grids composed of repeating irregular quadrilaterals that comprise four bpp and four Cu ions. The Cu1-bpp layer and Cu2-bpp layer are slightly different due to different conformations adopted by bpp. Each repeating irregular quadrilaterals of the Cu1-bpp layer has side lengths of 12.55 and 11.78 Å based on Cu1···Cu1 distances and angles of 80.2, 86.7, 96.4, and 96.4°, as shown in figure 4(b), while each of the repeating irregular quadrilaterals of Cu2-bpp layer has side lengths of 12.89 and 11.48 Å based on Cu2···Cu2 distances and angles of 77.7, 89.6, 96.0, and 96.0° in Cu2-bpp layer, as shown in figure 4(c). Sizes of the irregular quadrilaterals in both the Cu1-bpp and Cu2-bpp layer are large enough to allow Cu1-bpp layer to interpenetrate the Cu2-bpp layer. Indeed, the Cu1-bpp layer and Cu2-bpp layer in **2** interpenetrate each other within a plane and give a two-fold parallel interpenetrated 2-D double helical layer network (figure 4d), without the presence of solvent. Though bpp-based two-fold parallel interpenetrated 2-D networks were reported several years ago [18a, 22], studies on the 2-D interpenetrated networks with double helical structures are little explored [1e, 15a].

3.2. *Discussion on the synthesis and structures of 1 and 2*

Compound **1** is obtained from the reaction of $Zn(NO_3)_2 \cdot 6H_2O$, bpp, and sodium *p*-toluene sulfonate. Addition of $Cu(NO_3)_2 \cdot 3H_2O$ into the above system does not affect the formation of **1**. An effort to get an analog of **1** by reacting bpp and sodium *p*-toluene sulfonate with $Cu(NO_3)_2 \cdot 3H_2O$ instead of $Zn(NO_3)_2 \cdot 6H_2O$ has proved

a failure. Compound **2** is obtained from the reaction system of $Cu(NO_3)_2 \cdot 3H_2O$, NH_4SCN, and bpp. Addition of $Zn(NO_3)_2 \cdot 6H_2O$ into the system does not affect the formation of **2**. The results show that *p*-toluene sulfonates select Zn^{2+} rather than Cu^{2+} to coordinate in the system composed of $Zn(NO_3)_2 \cdot 6H_2O$, $Cu(NO_3)_2 \cdot 3H_2O$, bpp, and sodium *p*-toluene sulfonate to form **1**, while SCN^- and NO_3^- select Cu^{2+} rather than Zn^{2+} to coordinate in the system composed of $Zn(NO_3)_2 \cdot 6H_2O$, $Cu(NO_3)_2 \cdot 3H_2O$, bpp, and NH_4SCN, indicating that the ligand shows preference/selectivity when different types of metal ions are present at the same time. This may be helpful in designing new Cu-coordination polymers which are a very attractive subject [23]. Anionic ligands (*p*-$MeC_6H_5SO_3^-$, NO_3^-, and SCN^-) are monodentate in **1** and **2**, and there is no doubt that the coordination modes of the anionic ligands together with the flexible bpp are responsible for the formation of 2-D helical layer structures. Interpenetration occurred in **2** while not in **1** may be due to the steric hindrance of *p*-$MeC_6H_5SO_3^-$ that is too large to allow interpenetration between the 2-D helical double layers in **1** (figure 5), despite that the repeating meshes in **1** and **2** are large enough (figures 2b, 4b, and 4c) for interpenetration of the 2-D layers.

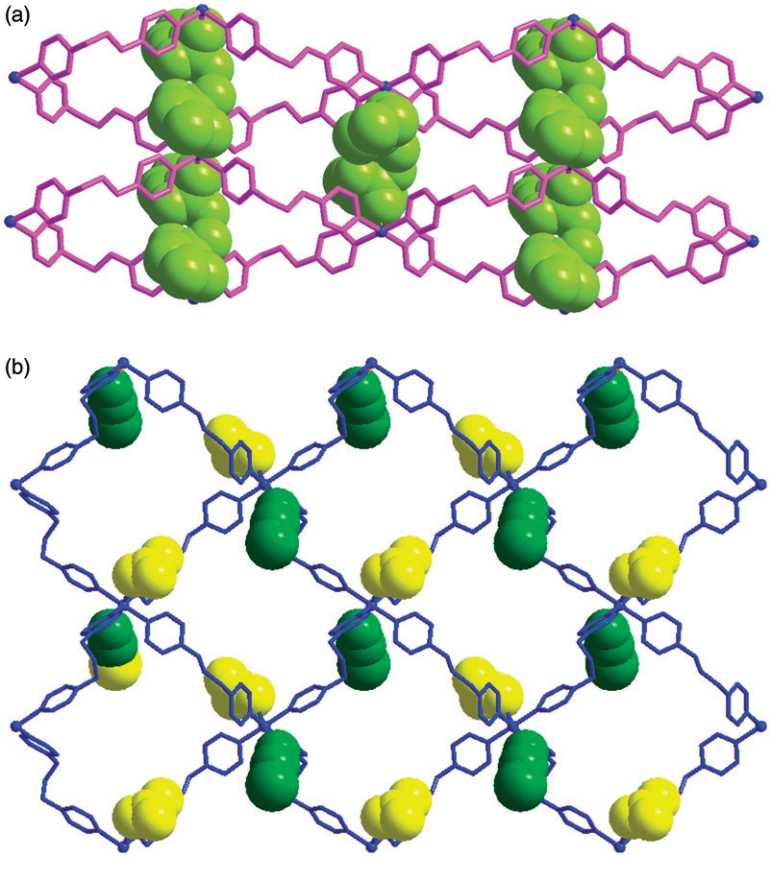

Figure 5. (Color online) The 2-D layers in **1** highlighting (in space-filling mode) the ionic ligands *p*-$MeC_6H_5SO_3^-$ (in pale green) coordinated to Zn^{2+} in **1** (a); the 2-D layers in **2** highlighting (in space-filling mode) the ionic ligands NO_3^- (in yellow) and SCN^- (in green) coordinated to Cu^{2+} in **2** (b).

We also make some comparison and analysis on closely relevant bpp-based metal-organic polymers in order to understand more the synthetic and structural regularity on bpp-based interpenetrated and helical structures. Besides the flexibility of bpp, which is the prerequisite for the formation of helical and/or interpenetrated structures, anionic ligands such as X^- (halides), SO_4^{2-}, and NCS^- are propitious to the formation of interpenetrated structures due to their small steric hindrance, while large solvent and neutral molecules filled in the crystal lattice sometimes prevent interpenetration. For example, the 2-D parallel interpenetrated network $[Cu_2(bpp)_4(NCS)_4]$ could be formed by using NCS^- as an anionic ligand [18a], the three-fold interpenetrated 3-D architecture $[Cu(bpp)_2Cl]Cl \cdot 1.5H_2O$ [18f] and four-fold interpenetrated diamond-like networks $[Cu(bpp)_2Cl_2] \cdot 2.75H_2O$ [18f] by using Cl^- as an anionic ligand were obtained, the compound $[Cu_2Br_2(bpp)_2]$ [15a] containing Br^- has a 2-D polycatenane formed by the interlocking of 1-D double-stranded tubular chains, while $[Cu_2I_2(bpp)_2] \cdot$(benzene) and $[Cu_2I_2(bpp)] \cdot$(naphthalene) [15a] both containing I^- possess only 1-D double-stranded tubular chains without interpenetration. Each empty space of the double-stranded 1-D chains in $[Cu_2I_2(bpp)_2] \cdot$(toluene) and $[Cu_2I_2(bpp)] \cdot$(naphthalene) is large enough and hosts a toluene or naphthalene guest, preventing the interpenetration of 1-D double-strand chains [15a]. Different solvents used in the reaction system may shed influence on structures and compositions of the resultant compounds, e.g., $[Cu_5(bpp)_8(SO_4)_4(EtOH)(H_2O)_5](SO_4) \cdot EtOH \cdot 25.5H_2O$ [18f] formed from a mixed solvent of water and ethanol possesses a unique 3-D polycatenated array in which the 1-D ribbons and the 2-D layers are entangled, while $[Cu_2(bpp)_2(HSO_4)_2] \cdot (SO_4) \cdot H_2O$ formed from DMF features a two-fold inclined interpenetrated 2-D (4, 4) net [18b]. The three-fold interpenetrated 3-D architecture $[Cu(bpp)_2Cl]Cl \cdot 1.5H_2O$ [18g] was obtained from water solution and the four-fold interpenetrated diamond-like networks $[Cu(bpp)_2Cl_2] \cdot 2.75H_2O$ [18g] were obtained from the ethanol solution.

The above analysis shows that the helicity/interpenetration of bpp-based compounds can be tuned and varied by simply varying the coordinating anions with different size and configuration. The strategy can be applied to design and synthesize helical/interpenetrated compounds based on any flexible ligands, including flexible organic carboxylic acids [20].

3.3. *Luminescent properties of 1*

The solid-state emission spectrum of **1** at room temperature is shown in the "Supplementary material." Compound **1** exhibits an intense broad photoluminescent emission centered at 415 nm ($\lambda_{exc} = 364$ nm). The photoluminescence of pure ligand is investigated to ascertain the emission band; *p*-toluenesulfonic acid sodium salt presents a weak emission at 345 nm and bpp gives a weak emission at 521 nm ($\lambda_{exc} = 400$ nm). Accordingly, the broad peak at 415 nm in **1** could be assigned to metal-to-ligand charge transfer or ligand-to-metal charge transfer [24].

3.4. *Thermogravimetric measurements*

In order to investigate the thermal properties of **1** and **2**, thermogravimetric analyses of **1** and **2** were carried out in air from 20°C to 1000°C and 20°C to 900°C, respectively. As shown in the "Supplementary material," the TGA curve of **1** shows the first weight

loss from 20°C to 448.55°C for the decomposition of two bpp (Found: 48.96%; Calcd: 49.56%). From 448.55°C to 1000°C about 42.33% weight loss is observed, which may correspond to the decomposition of two *p*-toluenesulfonates (Calcd: 42.56%). The weight loss processes are accompanied by one endothermal DTA peak at 217.47°C and one distinct exothermic DTA peak at 566.13°C.

The TGA curve of **2** (Supplementary material) shows the first weight loss from 20°C to 177.1°C for the decomposition of one NO_3^- (Found: 5.6%; Calcd: 5.34%). From 177.1°C to 533.7°C about 61.8% weight loss is observed, which may correspond to the decomposition of three bpp, one NO_3^-, and one NSC^- (Calcd 61.55%). In the third stage, it experiences a 22.38% weight loss from 533.7 to 594.8°C, which is attributed to the decomposition of one bpp and one NSC^- (Calcd 22.07%). From the DTA curve, it can be seen that the weight loss processes are accompanied by three distinct exothermic DTA peaks at 160.37°C, 205.37°C, and 567.86°C.

3.5. *XRD patterns*

The powder XRD patterns of **1** and **2** are in agreement with those simulated from X-ray single-crystal data, indicating the homogeneous phases of the final products (Supplementary material). No other peaks can be found in the pattern, revealing that there is no impurity in the products.

4. Conclusion

Preparation and characterization of two new transition metal-organic helical coordination polymers, **1** and **2**, are reported by using flexible bpp. Both **1** and **2** exhibit 2-D layer networks composed of alternate left-handed and right-handed bpp-containing helical chains, sharing Zn(II) in **1** and Cu(II) in **2**. Compound **1** exhibits a 2-D undulated double helical network and **2** exhibits a 2-fold parallel interpenetrated 2-D layer network. The difference is attributed to steric influence from the different anions because both compounds have bpp as the first ligand and their grids within the 2-D layers are large enough for interlayer interpenetration, i.e., the helicity and interpenetration can be tuned and varied by simply varying the coordinating anions with different size and configuration. Given a large number of flexible ligands, coordinating anions of various types and configurations as well as metal cations with preference/selectivity to ligands, new helical, or interpenetrated structures will be definitely synthesized if one applies the strategy by varying reaction conditions such as reagent ratio, pH, and temperature. Success will help with deeper understanding about the synthetic and structural regularity of resulting compounds with helical or interpenetrated structures and the inherent relationship between structure and emerging properties.

Supplementary material

Further details of the crystal structure determination have been deposited in the Cambridge Crystallographic Data Centre as supplementary publication. CCDC 848810

for **1** and CCDC 848811 for **2** contain the supplementary crystallographic data for this article.

Acknowledgments

The financial support from the National Natural Science Foundation of China (No. 20975009) is greatly acknowledged.

References

[1] (a) S.R. Fan, L.G. Zhu. *Inorg. Chem.*, **45**, 7935 (2006); (b) Y.W. Li, R.T. Yang. *J. Am. Chem. Soc.*, **128**, 726 (2006); (c) C.Y. Su, A.M. Goforth, M.D. Smith, P.J. Pellechia, H.C. Loye. *J. Am. Chem. Soc.*, **126**, 3576 (2004); (d) B. Kesanli, W.B. Lin. *Coord. Chem. Rev.*, **246**, 305 (2003); (e) L. Han, Y. Zhou, W.N. Zhao, X. Li, Y.X. Liang. *Cryst. Growth Des.*, **9**, 660 (2009); (f) J. Luo, Y. Zhao, H. Xu, T.L. Kinnibrugh, D. Yang,T.V. Timofeeva, L.L. Daemen, J. Zhang, W. Bao, J.D. Thompson, R.P. Currier. *Inorg. Chem.*, **46**, 9021 (2007); (g) J. Luo, M. Hong, R. Wang, R. Cao, L. Han, Z. Lin. *Eur. J. Inorg. Chem.*, 2705 (2003).
[2] (a) X.M. Gao, D.S. Li, J.J. Wang, F. Fu, Y.P. Wu, H.M. Hu, J. Wang. *CrystEngComm*, **10**, 479 (2008); (b) X. Shi, G.S. Zhu, S.L. Qiu, K.L. Huang, J.H. Yu, R.R. Xu. *Angew. Chem. Int. Ed.*, **43**, 6482 (2004); (c) M.L. Tong, X.L. Chen, S.R. Batten. *J. Am. Chem. Soc.*, **125**, 16170 (2003); (d) X.N. Chen, W.X. Zhang, X.M. Chen. *J. Am. Chem. Soc.*, **129**, 15738 (2007).
[3] (a) W.T. Chen, M.S. Wang, X. Liu, G.C. Guo, J.S. Huang. *Cryst. Growth Des.*, **6**, 2289 (2006); (b) L. Han, M.C. Hong. *Inorg. Chem. Commun.*, **8**, 406 (2005); (c) D.N. Dybtsev, H. Chun, S.H. Yoon, D. Kim, K. Kim. *J. Am. Chem. Soc.*, **126**, 1308 (2004); (d) D.R. Xiao, E.B. Wang, H.Y. An, Y.G. Li, L. Xu. *Cryst. Growth Des.*, **7**, 506 (2007).
[4] T.W. Bell, H. Jousselin. *Nature*, **367**, 441 (1994).
[5] (a) L. Han, Y. Zhou. *Inorg. Chem. Commun.*, **11**, 385 (2008); (b) L. Han, H. Valle, X.H. Bu. *Inorg. Chem.*, **46**, 1511 (2007).
[6] (a) S.Q. Zang, Y. Su, C.Y. Duan, Y.Z. Li, H.Z. Zhu, Q.J. Meng. *Chem. Commun.*, 4997 (2006); (b) E. Yang, J. Zhang, Z.J. Li, S. Gao, Y. Kang, Y.B. Chen, Y.H. Wen, Y.G. Yao. *Inorg. Chem.*, **43**, 6525 (2004); (c) Y.Q. Sun, J. Zhang, Y.M. Chen, G.Y. Yang. *Angew. Chem. Int. Ed.*, **44**, 5814 (2005); (d) R.H. Wang, Y.F. Zhou, Y.Q. Sun, D.Q. Yuan, L. Han, B.Y. Lou, B.L. Wu, M.C. Hong. *Cryst. Growth Des.*, **5**, 251 (2005).
[7] Y.W. Hu, G.H. Li, X.M. Liu, B. Hu, M.H. Bi, L. Gao, Z. Shi, S.H. Feng. *CrystEngComm*, **10**, 888 (2008).
[8] (a) E. Yang, J. Zhang, Z.J. Li, S. Gao, Y. Kang, Y.B. Chen, Y.H. Wen, Y.G. Yao. *Inorg. Chem.*, **43**, 6525 (2004); (b) S.Q. Zang, Y. Su, C.Y. Duan, Y.Z. Li, H.Z. Zhu, Q.J. Meng. *Chem. Commun.*, 4997 (2006).
[9] A. Jouaiti, M.W. Hosseini, N. Kyritsakas, P. Grosshans, J.M. Planeix. *Chem. Commun.*, 3078 (2006).
[10] (a) X.R. Hao, X.L. Wang, C. Qin, Z.M. Su, E.B. Wang, Y.Q. Lan, K.Z. Shao. *Chem. Commun.*, 4620 (2007); (b) E.V. Anokhina, Y.B. Go, Y. Lee, T. Vogt, A.J. Jacobson. *J. Am. Chem. Soc.*, **128**, 9957 (2006); (c) X.L. Wang, C. Qin, E.B. Wang, L. Xu, Z.M. Su, C.W. Hu. *Angew. Chem. Int. Ed.*, **43**, 5036 (2004).
[11] (a) L. Han, M.C. Hong, R.H. Wang, J.H. Luo, Z.Z. Lin, D.Q. Yuan. *Chem. Commun.*, 2580 (2003); (b) P.A. Maggard, C.L. Stern, K.R. Poeppelmeier. *J. Am. Chem. Soc.*, **123**, 7742 (2001); (c) Y.H. Feng, Y. Guo, Y.O. Yang, Z.Q. Liu, D.Z. Liao, P. Cheng, S.P. Yan, Z.H. Jiang. *Chem. Commun.*, 3643 (2007).
[12] (a) Y.W. Hu, G.H. Li, X.M. Liu, B. Hu, M.H. Bi, L. Gao, Z. Shi, S.H. Feng. *CrystEngComm*, **10**, 888 (2008); (b) L.F. Ma, L.Y. Wang, Y.Y. Wang, M. Du, J.G. Wang. *CrystEngComm*, **11**, 109 (2009); (c) X.Y. Cao, Z.J. Li, J. Zhang, Y.Y. Qin, J.K. Cheng, Y.G. Yao. *CrystEngComm*, **10**, 1345 (2008).
[13] X.H. Geng, Y.L. Feng, Y.Z. Lan. *Inorg. Chem. Commun.*, **12**, 447 (2009).
[14] (a) L. Carlucci, G. Ciani, D.M. Proserpio, S. Rizzato. *CrystEngComm*, **4**, 413 (2002); (b) L. Carlucci, G. Ciani, D.M. Proserpio, S. Rizzato. *CrystEngComm*, **4**, 121 (2002).
[15] (a) S. Hu, A.J. Zhou, Y.H. Zhang, S. Ding, M.L. Ton. *Cryst. Growth Des.*, **6**, 2543 (2006); (b) C.J. Wang, Y.Y. Wang, J.Q. Liu, H. Wang, Q.Z. Shi, S.M. Peng. *Inorg. Chim. Acta*, **362**, 543 (2009); (c) C.X. Meng, D.S. Li, J. Zhao, F. Fu, X.N. Zhang, L. Tang, Y.Y. Wang. *Inorg. Chem. Commun.*, **12**, 793 (2009).
[16] D.M. Proserpio, R. Hoffman, P. Preuss. *J. Am. Chem. Soc.*, **116**, 9634 (1994).

[17] (a) J.S. Miller. *Adv. Mater.*, **13**, 525 (2001); (b) O. Ermer. *Adv. Mater.*, **3**, 608 (1991).
[18] (a) R.A. Farani, W.M. Teles, C.B. Pinheiro, K.J. Guedes, K. Krambrock, M.I. Yoshida, L.F.C. Oliveira, F.C. Machado. *Inorg. Chim. Acta*, **361**, 2045 (2008); (b) F. Luo, Y.X. Che, J.M. Zheng. *J. Mol. Struct.*, **828**, 162 (2007); (c) G.H. Wang, Z.G. Li, H.Q. Jia, N.H. Hu, J.W. Xu. *Cryst. Growth Des.*, **8**, 1932 (2008); (d) S. Hu, C. Chen, M.L. Tong, B. Wang, Y.X. Yan, S.R. Batten. *Angew. Chem. Int. Ed.*, **44**, 5471 (2005); (e) J.Q. Liu, Y.Y. Wang, P. Liu, W.P. Wu, Y.P. Wu, X.R. Zeng, F. Zhong, Q.Z. Shi. *Inorg. Chem.*, **10**, 343 (2007); (f) L. Carlucci, G. Ciani, M. Moret, D.M. Proserpio, S. Rizzato. *Angew. Chem. Int. Ed.*, **39**, 1506 (2000); (g) L. Carlucci, G. Ciani, M. Moret, D.M. Proserpio, S. Rizzato. *Chem. Mater.*, **14**, 12 (2002).
[19] G.M. Sheldrick. *SHELXL97, SHELXS97, Program for X-ray Crystal Structure Solution and Refinement*, University of Göttingen, Göttingen, Germany (1997).
[20] (a) J.F. Song, R.S. Zhou, T.P. Hu, Z. Chen. *J. Coord. Chem.*, **63**, 4201 (2010); (b) H.J. Hao, C.W. Lin, X.H. Yin, F. Zhang. *J. Coord. Chem.*, **64**, 965 (2011); (c) S.M. Fang, D.L. Peng, M. Chen, L.R. Jia, M. Hu. *J. Coord. Chem.*, **65**, 668 (2012); (d) L.J. Chen, X.Y. Wu, Q.G. Zhai, Z.G. Zhao, Q.S. Zhang, C.Z. Lu. *Inorg. Chem. Commun.*, **10**, 1457 (2007).
[21] (a) W. Lewis, P.J. Steel. *J. Coord. Chem.*, **64**, 115 (2011); (b) P. Pachfule, R. Das, P. Poddar, R. Banerjee. *Cryst. Growth Des.*, **11**, 1215 (2011); (c) G.Q. Kong, C.D. Wu. *Cryst. Growth Des.*, **10**, 4590 (2010); (d) G.B. Li, H.C. Fang, Y.P. Cai, Z.Y. Zhou, P. Thallapally, J. Tian. *Inorg. Chem.*, **49**, 7241 (2010).
[22] (a) E.Q. Gao, Y.X. Xu, A.L. Cheng, M.Y. He, C.H. Yan. *Inorg. Chem. Commun.*, **9**, 212 (2006); (b) Y. Kang, J. Zhang, Y.Y. Qin, Z.J. Li, Y.G. Yao. *J. Mol. Struct.*, **827**, 126 (2007).
[23] J.Y. Lu. *Coord. Chem. Rev.*, **246**, 327 (2003).
[24] Y.M. Dai, E. Tang, J.F. Huang, Y.G. Yao, X.D. Huang. *J. Mol. Struct.*, **918**, 183 (2009).